UNCLASSIFIED

SECURITY CLASSIFICATION OF THIS PAGE

AD-A217 792

REPORT DOCUMENTATION PAGE

Form Approved
OMB No. 0704-0188

1a. REPORT SECURITY CLASSIFICATION Unclassified	1b. RESTRICTIVE MARKINGS
2a. SECURITY CLASSIFICATION AUTHORITY	3. DISTRIBUTION/AVAILABILITY OF REPORT Approved for public release; distribution unlimited.
2b. DECLASSIFICATION/DOWNGRADING SCHEDULE	
4. PERFORMING ORGANIZATION REPORT NUMBER(S) HDL-TR-2169	5. MONITORING ORGANIZATION REPORT NUMBER(S)
6a. NAME OF PERFORMING ORGANIZATION Harry Diamond Laboratories 6b. OFFICE SYMBOL (If applicable) SLCHD-ST-AP	7a. NAME OF MONITORING ORGANIZATION
6c. ADDRESS (City, State, and ZIP Code) 2800 Powder Mill Road Adelphi, MD 20783-1197	7b. ADDRESS (City, State, and ZIP Code)
8a. NAME OF FUNDING/SPONSORING ORGANIZATION U.S. Army Laboratory Command 8b. OFFICE SYMBOL (If applicable) AMSLC	9. PROCUREMENT INSTRUMENT IDENTIFICATION NUMBER
8c. ADDRESS (City, State, and ZIP Code) 2800 Powder Mill Road Adelphi, MD 20783-1145	10. SOURCE OF FUNDING NUMBERS PROGRAM ELEMENT NO. 6.2120.A; PROJECT NO. AH25; TASK NO.; WORK UNIT ACCESSION NO.

11. TITLE (Include Security Classification)
Crystallography, Spectroscopic Analysis, and Lasing Properties of Nd^{3+}: $Y_3Sc_2Al_3O_{12}$

12. PERSONAL AUTHOR(S)
Toomas H. Allik, Clyde A. Morrison, John B. Gruber, and Milan R. Kokta

13a. TYPE OF REPORT	13b. TIME COVERED	14. DATE OF REPORT (Year, Month, Day)	15. PAGE COUNT
Final	FROM Aug 88 TO Dec 88	December 1989	24

16. SUPPLEMENTARY NOTATION
AMS code: AH25, HDL project: R8A951

17. COSATI CODES		
FIELD	GROUP	SUB-GROUP
20	02	
20	05	

18. SUBJECT TERMS (Continue on reverse if necessary and identify by block number)
Yttrium scandium aluminum garnet, neodymium, crystallography, refractive index, diode pumped laser, crystal-field parameters, Judd-Ofelt parameters, branching ratios, Neodymium(3+), (5G)

19. ABSTRACT (Continue on reverse if necessary and identify by block number)
The crystallographic, optical, and spectroscopic properties of Nd^{3+}:$Y_3Sc_2Al_3O_{12}$ are reported from which an assessment can be made regarding the material's potential as a laser. Individual Stark levels for many of the $^{(2S+1)}L_J$ manifolds of Nd^{3+} $(4f^3)$ in the crystal have been identified from emission and absorption data up to 17,600 cm^{-1} at 14 K. The observed crystal-field splitting and the measured cross sections (intensities) associated with manifold-to-manifold transitions are compared with calculated splittings and calculated intensities. Branching ratios and diode-array-pumped laser slope efficiencies are also reported. We conclude that Nd:YSAG has potential as a diode-pumped 1 μm laser material.

Keywords: micrometer

20. DISTRIBUTION/AVAILABILITY OF ABSTRACT	21. ABSTRACT SECURITY CLASSIFICATION
☒ UNCLASSIFIED/UNLIMITED ☐ SAME AS RPT. ☐ DTIC USERS	Unclassified
22a. NAME OF RESPONSIBLE INDIVIDUAL Clyde A. Morrison	22b. TELEPHONE (Include Area Code) (202) 394-2042
	22c. OFFICE SYMBOL SLCHD-ST-AP

DD Form 1473, JUN 86 Previous editions are obsolete.

SECURITY CLASSIFICATION OF THIS PAGE
UNCLASSIFIED

The findings in this report are not to be construed as an official Department of the Army position unless so designated by other authorized documents.

Citation of manufacturer's or trade names does not constitute an official endorsement or approval of the use thereof.

Destroy this report when it is no longer needed. Do not return it to the originator.

UNCLASSIFIED

SECURITY CLASSIFICATION OF THIS PAGE

REPORT DOCUMENTATION PAGE

Form Approved OMB No. 0704-0188

1a. REPORT SECURITY CLASSIFICATION Unclassified	1b. RESTRICTIVE MARKINGS
2a. SECURITY CLASSIFICATION AUTHORITY	3. DISTRIBUTION/AVAILABILITY OF REPORT Approved for public release; distribution unlimited.
2b. DECLASSIFICATION/DOWNGRADING SCHEDULE	
4. PERFORMING ORGANIZATION REPORT NUMBER(S) HDL-TR-2169	5. MONITORING ORGANIZATION REPORT NUMBER(S)
6a. NAME OF PERFORMING ORGANIZATION Harry Diamond Laboratories 6b. OFFICE SYMBOL (If applicable) SLCHD-ST-AP	7a. NAME OF MONITORING ORGANIZATION
6c. ADDRESS (City, State, and ZIP Code) 2800 Powder Mill Road Adelphi, MD 20783-1197	7b. ADDRESS (City, State, and ZIP Code)
8a. NAME OF FUNDING/SPONSORING ORGANIZATION U.S. Army Laboratory Command 8b. OFFICE SYMBOL (If applicable) AMSLC	9. PROCUREMENT INSTRUMENT IDENTIFICATION NUMBER
8c. ADDRESS (City, State, and ZIP Code) 2800 Powder Mill Road Adelphi, MD 20783-1145	10. SOURCE OF FUNDING NUMBERS PROGRAM ELEMENT NO. 6.2120.A; PROJECT NO. AH25; TASK NO.; WORK UNIT ACCESSION NO.

11. TITLE (Include Security Classification)

Crystallography, Spectroscopic Analysis, and Lasing Properties of Nd^{3+}: $Y_3Sc_2Al_3O_{12}$

12. PERSONAL AUTHOR(S)

Toomas H. Allik, Clyde A. Morrison, John B. Gruber, and Milan R. Kokta

13a. TYPE OF REPORT	13b. TIME COVERED	14. DATE OF REPORT (Year, Month, Day)	15. PAGE COUNT
Final	FROM Aug 88 TO Dec 88	December 1989	24

16. SUPPLEMENTARY NOTATION

AMS code: AH25, HDL project: R8A951

17. COSATI CODES		
FIELD	GROUP	SUB-GROUP
20	02	
20	05	

18. SUBJECT TERMS (Continue on reverse if necessary and identify by block number)

Yttrium scandium aluminum garnet, neodymium, crystallography, refractive index, diode pumped laser, crystal-field parameters, Judd-Ofelt parameters, branching ratios

19. ABSTRACT (Continue on reverse if necessary and identify by block number)

The crystallographic, optical, and spectroscopic properties of Nd^{3+}:$Y_3Sc_2Al_3O_{12}$ are reported from which an assessment can be made regarding the material's potential as a laser. Individual Stark levels for many of the $^{2S+1}L_J$ manifolds of Nd^{3+} ($4f^3$) in the crystal have been identified from emission and absorption data up to 17,600 cm^{-1} at 14 K. The observed crystal-field splitting and the measured cross sections (intensities) associated with manifold-to-manifold transitions are compared with calculated splittings and calculated intensities. Branching ratios and diode-array-pumped laser slope efficiencies are also reported. We conclude that Nd^{3+}:YSAG has potential as a diode-pumped 1 μm laser material.

20. DISTRIBUTION/AVAILABILITY OF ABSTRACT	21. ABSTRACT SECURITY CLASSIFICATION
☒ UNCLASSIFIED/UNLIMITED ☐ SAME AS RPT. ☐ DTIC USERS	Unclassified
22a. NAME OF RESPONSIBLE INDIVIDUAL Clyde A. Morrison	22b. TELEPHONE (Include Area Code) (202) 394-2042
	22c. OFFICE SYMBOL SLCHD-ST-AP

DD Form 1473, JUN 86 *Previous editions are obsolete.*

SECURITY CLASSIFICATION OF THIS PAGE

UNCLASSIFIED

Contents

Figures

Tables

1. Introduction

Increasing demands placed on solid-state lasers in applications ranging from communications to medicine highlight the need to develop new materials that have better diode pump laser characteristics than the standard laser material Nd:YAG [1–9]. The challenge is made clear with the present availability of single laser diodes with powers exceeding 1 W and two-dimensional arrays producing fluxes of more than 4 kW/cm^2 at the required wavelength. Desirable properties of new diode-pumped Q-switched solid-state lasers include a longer fluorescent lifetime and a larger absorption coefficient than is possible with Nd:YAG. In addition, the optical, mechanical, and thermal crystal properties of the host must be competitive with Nd:YAG to permit high-repetition-rate applications.

There are several reasons for examining the laser properties of Nd:$Y_3Sc_2Al_3O_{12}$ (YSAG) in greater detail [10–12]. The distribution coefficient for Nd^{3+} in YSAG is roughly twice that for YAG [13,14], making it possible to increase the Nd^{3+} concentration in YSAG over that in YAG. Replacing Al^{3+} ions with larger Sc^{3+} ions increases the distance between dodecahedral lattice sites (substitutional sites for Nd^{3+} ions in the garnet structure). Any increase in separation between neighboring Nd^{3+} ions, especially with increasing concentration, tends to reduce the relatively strong ion/ion interaction in YAG, which leads to concentration quenching of the Nd^{3+} fluorescence [10,15,16]. In addition, the aluminum-based systems, such as YAG, YSAG, or gadolinium scandium aluminum garnet (GSAG), are formed from more stable constituent oxides than gallium-containing materials, such as gadolinium scandium gallium garnet (GSGG). The tendency for color center formation in gallium-containing garnets is due to oxidation state variation or oxygen vacancies, and this problem is greatly reduced in aluminate systems.

Only some of the spectroscopic properties of Nd:YSAG have been reported in the open literature [10,17]. Kaminskii reports energy levels up to the $^4F_{3/2}$ manifold only [10]. Most of the literature concentrates on the empirical evaluation of Nd:YSAG and Cr^{3+} sensitized Nd:YSAG as a laser [11,12,18,19]. However, to fully assess the potential of this material, it is important to study the spectroscopic properties in greater detail. The individual experimental Stark levels and the measured cross sections and lifetimes of transitions between these levels should be compared with theoretical predictions based on lattice-sum calculations, crystal-field splitting, and the predicted cross sections and lifetimes based on the Judd-Ofelt model for rare-earth ions in solids [16,20–22].

We report here the results of crystal growth and x-ray diffraction studies, along with measurements on the index of refraction of Nd:YSAG. The experimental Stark levels for many of the $^{2S+1}L_J$ manifolds of Nd^{3+} ($4f^3$) deduced from both absorption and emission data are tabulated up to 17,600 cm^{-1} and compared with a theoretical crystal-field splitting calculation. A survey spectrum of Nd:YSAG between 300 and 1000 nm and the fluorescence from $^4F_{3/2}$ to $^4I_{11/2}$, both obtained at room temperature, provide a general overview of observed optical properties of Nd^{3+}. Absorption intensities from the ground-state manifold of Nd^{3+} ($^4I_{9/2}$) to excited manifolds observed in the survey spectrum are compared with calculated intensities based on the Judd-Ofelt theory [20–22]. Branching ratios and slope efficiencies are also reported from which an assessment can be made regarding Nd:YSAG as a laser material.

2. Experimental Results and Discussion

2.1 Crystal Growth and Structure

Yttrium scandium aluminum garnet belongs to the group of oxide compounds crystallizing in garnet structure. The first garnet containing scandium was synthesized by Moro-

nova and Feofilov [23], and a systematic study of Sc incorporation into aluminum garnets was made by Kokta [13] in 1973. Subsequently, a scandium-substituted rare-earth aluminum garnet (GSAG) was grown by Brandle and Vanderleeden [24]. An interest in scandium-substituted garnets was revived a decade later when their usefulness as tunable solid-state laser hosts was demonstrated with Cr^{3+} doped in GSGG [25].

The first crystals of yttrium scandium aluminum garnets doped with either neodymium or chromium were grown in a 2 in. × 2 in. crucible. They were approximately 0.9 in. in diameter and 2 in. long. These crystals were used to fabricate spectroscopic samples as well as seeds for further crystal growth.

For laser application, a 5-in.-long Nd-doped crystal of 1.5-in. diameter was grown. The furnace used to grow this material was built from a silica sleeve inserted in an rf coil. A 3 in. × 3 in. iridium crucible was used which was surrounded by a 3.5-in. I.D. zirconium oxide liner. The space between the ZrO_2 liner and the SiO_2 sleeve was filled with insulation consisting of zirconium oxide bubbles (grog). The induction coil, which was made from 3/8-in.-diameter copper tubing, was wound into 12 turns around the growth furnace, and powered by a 50-kW motor generator operating at a 10-kHz frequency. The crucible was filled in the 3:2:3 molar ratio for Y_2O_3, Sc_2O_3, and Al_2O_3. The amount of Nd_2O_3 was calculated for substitution of 1.5-percent Nd into eightfold coordination sites, under the assumption that the Nd distribution coefficient, k_{Nd}, approached 0.4 in this system. However, the Nd concentration of a spectroscopic sample from the boule was determined by x-ray fluorescence to be 1.76 ± 0.10 at. wt.%, which corresponds to an Nd density of $(3.33 \pm 0.07) \times 10^{19}$ cm^{-3} [26]. The deviation between the measured and calculated Nd concentration is not surprising, since the exact value of k_{Nd} is a growth-dependent parameter (rotation rate, pull rate). More growth runs would be required to determine k_{Nd} precisely for given growth conditions.

The crystals were grown along the <111> orientation, at a rate of 0.015 in./hour, and were rotated at 15 rpm. They were grown under an ambient atmosphere of nitrogen containing 800 ppm by volume of O_2. The melting point was determined with an optical pyrometer to be 1900 ± 25°C, uncorrected for emissivity. YSAG showed typical garnet faceting as observed in YAG crystals. The interface shape was convex, and strain was observed in the "core" area. No attempts were made to change the interface shape. The strain pattern is significantly more pronounced in YSAG than is the strain in YAG. YSAG crystals have a much higher tendency to crack, and therefore extreme caution must be exercised during their fabrication. Contrary to the findings of Brandle [24], a slower pull rate seems to ease this problem, and rates even lower than 0.015 in./hr may be well justified, especially for crystals doped with Nd.

The crystal structure analysis was performed on an automated Nicolet R3m/μ diffractometer equipped with an incident-beam graphite monochromator and Mo K_α radiation (λ = 0.7107 Å). Single-crystal diffraction patterns of the crystal showed that the crystals were cubic, belonging to the space group $Ia\bar{3}d$ (No. 230), with a unit cell axis length of a = 12.271 Å (V = 1847.6 Å^3). The lattice parameter differs from that of Kokta [13] (a = 12.324 Å) and Bogomolova [27] (a = 12.251 Å); this difference is attributed to the distribution coefficient for Sc being less than unity, which allows for mixed occupancy between Sc and Al in the octahedral site. This should allow ranges in lattice parameters from stoichiometric YSAG (a = 12.32 Å) to YAG (a = 12.00 Å). Elemental analysis performed on the sample by x-ray fluorescence did indeed show lower Sc than expected in the crystal [26]. The 191 independent single-crystal reflections recorded were used to refine the structure by least squares to residuals of R = 0.0342 and wR = 0.0502. Positional and thermal parameters are listed in table 1. Further details on the data collection and on the crystal structure are given by Campana [28].

Table 1. Atom coordinates ($\times 10^4$) and thermal coefficients ($Å^2 \times 10^3$) of $Y_3Sc_2Al_3O_{12}$
Parenthetical values are estimated standard deviations.

Atom	x	y	z	U[a]
Y	0	0	0	74 (4)
Sc	0	2500	1250	51 (3)
Al	0	2500	3750	41 (7)
O	309 (3)	562 (3)	6562 (3)	67 (9)

[a]Equivalent isotropic U defined as one third of the trace of the orthogonalized U_{ij} tensor.

2.2 Index of Refraction

The refractive indices of Nd:YSAG were measured using the method of minimum deviation [29]. A polished prism of Nd:YSAG was fabricated to a height of 5 mm and had faces of 12 and 17 mm. The prism angle was 44°55′. A Spencer 2754 Spectrometer (American Optical Company) was used to make all angular measurements, and multiline argon ion and helium neon lasers were used as light sources between 457.9 and 632.8 nm. The measured refractive indices are given in table 2. The accuracy of these measurements was ±0.002 because of the poor optical quality of the sample.

These experimental data were least-squares fit to Sellmeier's dispersion equation

$$[n(\lambda)]^2 = 1 + \frac{A\lambda^2}{\lambda^2 - B} \qquad (1)$$

where $A = 2.420 \pm 0.008$ and $B = 0.01520 \pm 0.00064\ \mu m^2$. These results agree well with the results of Wemple and Tabor for undoped YSAG [30]. The refractive indices for the doped sample are higher than the ones for the undoped.

Table 2. Measured and calculated indices of refraction of Nd^{3+}:$Y_3Sc_2Al_3O_{12}$ at 298 K

Wavelength	n_{meas}	n_{calc}
457.9	1.900	1.900
476.5	1.895	1.896
488.0	1.893	1.893
496.5	1.891	1.892
514.5	1.889	1.889
594.5	1.880	1.878
611.9	1.878	1.877
632.8	1.873	1.875

Crystal	Sellmeier coefficients	
	A	B
Nd:YSAG	2.420	0.01520
YSAG[a]	2.4118	0.01477

[a]Reference 30.

2.3 Nd^{3+} Absorption

The absorption spectrum of neodymium-doped YSAG was investigated in the range from 1,500 to 40,000 cm^{-1}. These data were recorded in the ultraviolet, visible, and infrared on Perkin-Elmer Lambda 9 and 983G spectrometers interfaced to the Perkin-Elmer 7500 computer. Figure 1 shows the room-temperature absorption spectrum between 300 and 1000 nm of a 2.95-mm-long, Nd^{3+}:YSAG sample with the Fresnel reflection losses removed.

Determination of the individual Stark levels of the Nd^{3+} ions in the dodecahedral sites (D_2 symmetry) was accomplished by cooling the sample to cryogenic temperatures. A closed-cycle refrigerator, CTI-Cryogenics Model 21, was used to obtain spectra at 14 K. Table 3 lists the 60 lowest experimentally determined energy levels (up to 17,600 cm^{-1}). Energy levels up to 40,000 cm^{-1} have been determined and are currently being fit to a theoretical crystal-field calculation which includes spin-correlation effects; this calculation will be reported at a later date [31]. The low-lying energy levels, up to $^4F_{3/2}$, agree very well with those of Kaminskii [10]. The overall accuracy of the measurements is ≤5 cm^{-1}.

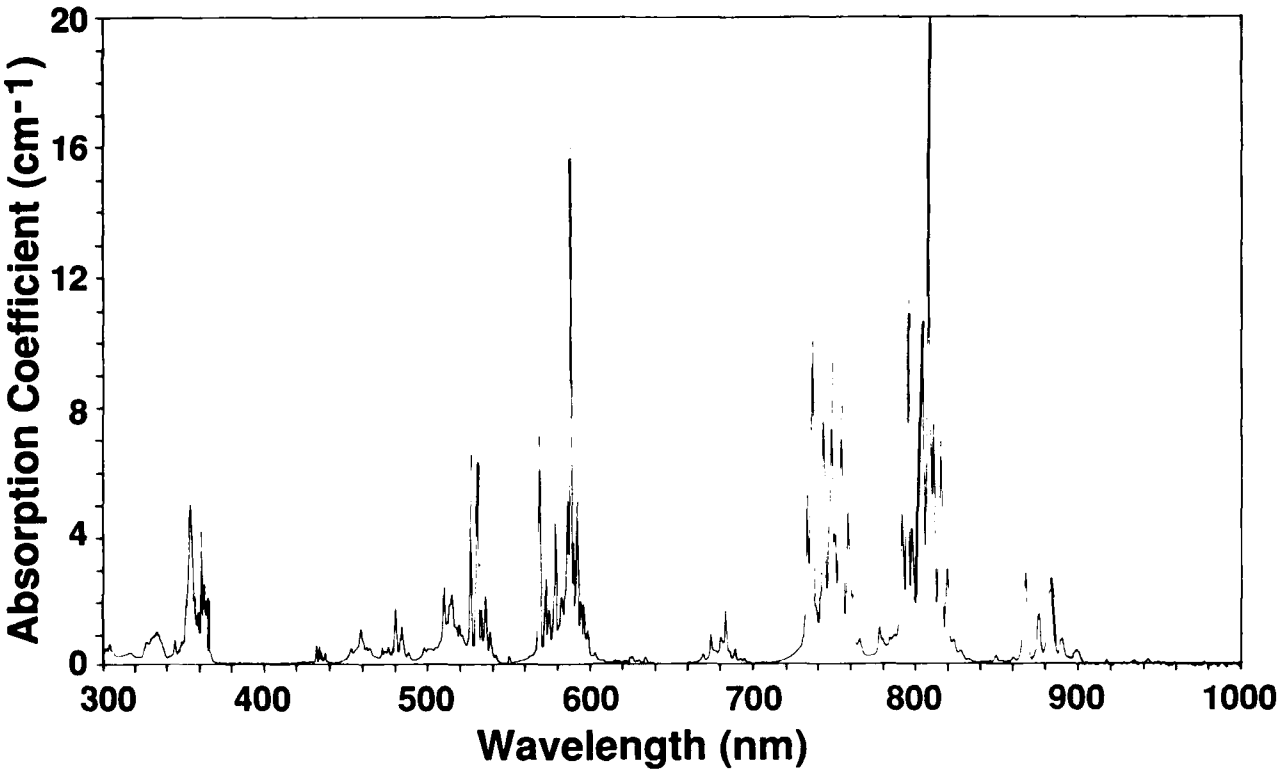

Figure 1. Room-temperature absorption spectrum of Nd^{3+}:YSAG. Nd concentration is 3.3×10^{19} cm^{-3}.

2.4 Nd^{3+} Fluorescence

The fluorescence spectrum of Nd^{3+}:YSAG was recorded with a Spex F222 spectrometer equipped with a North Coast model EO-817L Ge detector. Figure 2 shows the fluorescence of Nd^{3+}:YSAG and, for comparison, Nd^{3+}:YAG in the region of the ${}^4F_{3/2} \rightarrow {}^4I_{11/2}$ ($R_{1,2} \rightarrow Y_{1-6}$) transitions. In general, the fluorescence lines of Nd:YSAG show a broadening versus YAG. At room temperature, the two most intense lines for Nd:YSAG appear at 1.0622 and 1.0595 μm. These wavelengths correspond to the $R_2 \rightarrow Y_3$ and $R_1 \rightarrow Y_1$ transitions, respectively. In addition to these two prominent lines, the $R_1 \rightarrow Y_2$ and $R_2 \rightarrow Y_4$ transitions appear as shoulders on the long-wavelength side of the band. The individual Stark-level branching ratios were estimated from the peak heights to be 15 percent for $R_2 \rightarrow Y_3$ and 13 percent for $R_1 \rightarrow Y_1$. Accurate determinations of the distributions were not possible because of the limited resolution of the monochromator.

The fluorescence lifetime of the ${}^4F_{3/2}$ state was measured using a GaAlAs laser diode as the excitation source. The diode emits radiation at 805 nm at room temperature, and the pulse duration was 2 μs. Fluorescence detection was viewed through an 850-nm long-pass filter into an Si detector. Signals were processed by a Stanford Research Systems boxcar integrator and stored in a computer. The fluorescence lifetime at room temperature was 208 ± 5 μs at an Nd concentration of 1.76 at. wt.%. A comparable Nd concentration in YAG would have a lifetime of 160 μs [10].

Table 3. Experimental and theoretical crystal-field splittings of Nd^{3+} ion manifolds in YSAG

	Energy		$^{2S+1}L_J$ (centroid, cm^{-1})	Free ion mixture (%)
	Exp	Theo		
1	0	−11		$98.18\,{}^4I_{9/2} + 1.40\,{}^4I_{11/2} + 0.27\,{}^4I_{13/2}$
2	114	120	$^4I_{9/2}$	$98.08\,{}^4I_{9/2} + 1.38\,{}^4I_{11/2} + 0.39\,{}^4I_{13/2}$
3	183	188	(362)	$96.68\,{}^4I_{9/2} + 3.06\,{}^4I_{11/2} + 0.09\,{}^4I_{13/2}$
4	301	300		$95.70\,{}^4I_{9/2} + 4.06\,{}^4I_{11/2} + 0.07\,{}^4F_{3/2}$
5	823	824		$97.68\,{}^4I_{9/2} + 2.04\,{}^4I_{11/2} + 0.20\,{}^4I_{13/2}$
6	1979	1982		$96.98\,{}^4I_{11/2} + 2.31\,{}^4I_{13/2} + 0.30\,{}^4I_{15/2}$
7	2022	2016	$^4I_{11/2}$	$95.12\,{}^4I_{11/2} + 2.77\,{}^4I_{13/2} + 1.81\,{}^4I_{9/2}$
8	2101	2104	(2222)	$96.78\,{}^4I_{11/2} + 2.07\,{}^4I_{13/2} + 0.77\,{}^4I_{9/2}$
9	2136	2131		$96.82\,{}^4I_{11/2} + 2.47\,{}^4I_{13/2} + 0.42\,{}^4I_{9/2}$
10	2437	2442		$93.83\,{}^4I_{11/2} + 4.38\,{}^4I_{9/2} + 1.58\,{}^4I_{13/2}$
11	2495	2495		$95.11\,{}^4I_{11/2} + 4.10\,{}^4I_{9/2} + 0.61\,{}^4I_{13/2}$
12	3905	3906		$97.08\,{}^4I_{13/2} + 2.48\,{}^4I_{15/2} + 0.14\,{}^4I_{11/2}$
13	3929	3923	$^4I_{13/2}$	$95.92\,{}^4I_{13/2} + 2.34\,{}^4I_{15/2} + 1.42\,{}^4I_{11/2}$
14	4029	4036	(4188)	$97.90\,{}^4I_{13/2} + 1.33\,{}^4I_{15/2} + 0.35\,{}^4I_{11/2}$
15	4044	4042		$96.58\,{}^4I_{13/2} + 2.36\,{}^4I_{15/2} + 0.67\,{}^4I_{11/2}$
16	4057[a]	4411		$96.20\,{}^4I_{13/2} + 2.88\,{}^4I_{11/2} + 0.53\,{}^4I_{15/2}$
17	4419	4420		$94.25\,{}^4I_{13/2} + 3.25\,{}^4I_{11/2} + 2.16\,{}^4I_{15/2}$
18	4478	4478		$95.96\,{}^4I_{13/2} + 2.76\,{}^4I_{11/2} + 0.91\,{}^4I_{15/2}$
19	5766	5772		$97.68\,{}^4I_{15/2} + 1.95\,{}^4I_{15/2} + 0.10\,{}^4F_{9/2}$
20	5797	5794		$99.08\,{}^4I_{15/2} + 0.51\,{}^4I_{13/2} + 0.13\,{}^4F_{9/2}$
21	5927	5924	$^4I_{15/12}$	$98.75\,{}^4I_{15/2} + 0.77\,{}^4I_{13/2} + 0.14\,{}^4F_{9/2}$
22	5981	5988	(6221)	$98.57\,{}^4I_{15/2} + 0.85\,{}^4I_{13/2} + 0.21\,{}^4F_{9/2}$
23	6544	6539		$97.20\,{}^4I_{15/2} + 2.48\,{}^4I_{13/2} + 0.08\,{}^4I_{11/2}$
24	6560	6563		$98.48\,{}^4I_{15/2} + 1.03\,{}^4I_{13/2} + 0.43\,{}^4I_{11/2}$
25	6622	6625		$97.56\,{}^4I_{15/2} + 2.12\,{}^4I_{13/2} + 0.13\,{}^4I_{11/2}$
26	6711	6704		$97.42\,{}^4I_{15/2} + 2.24\,{}^4I_{13/2} + 0.25\,{}^4F_{7/2}$
27	11,423	11,431	$^4F_{3/2}$	$93.77\,{}^4F_{3/2} + 2.80\,{}^4F_{5/2} + 1.35\,{}^2H_{9/2}$
28	11,523	11,515	(11,523)	$93.44\,{}^4F_{3/2} + 3.54\,{}^4F_{5/2} + 1.45\,{}^4F_{7/2}$
29	12,382	12,367	$^4F_{5/2}$	$77.45\,{}^4F_{5/2} + 13.84\,{}^2H_{9/2} + 3.96\,{}^4F_{7/2}$
30	12,441	12,435	(12,524)	$61.74\,{}^2H_{9/2} + 32.80\,{}^4F_{5/2} + 3.17\,{}^4F_{3/2}$
31	12,538[a]	12,456		$65.56\,{}^2H_{9/2} + 29.23\,{}^4F_{5/2} + 2.90\,{}^4F_{3/2}$
32	12,583	12,590		$75.52\,{}^2H_{9/2} + 23.52\,{}^4F_{5/2} + 0.20\,{}^4F_{3/2}$
33	12,621	12,633		$95.97\,{}^4F_{5/2} + 2.41\,{}^2H_{9/2} + 0.62\,{}^4F_{7/2}$
34	12,637[a]	12,690	$^2H_{9/2}$	$88.30\,{}^2H_{9/2} + 10.59\,{}^4F_{5/2} + 0.29\,{}^2H_{11/2}$
35	12,825	12,817	(12,664)	$92.38\,{}^2H_{9/2} + 6.91\,{}^4F_{5/2} + 0.17\,{}^4F_{3/2}$
36	12,860	12,869		$93.27\,{}^2H_{9/2} + 5.82\,{}^4F_{5/2} + 0.18\,{}^2H_{11/2}$

[a]Expermental energy levels not used in the crystal-field calculations.

Table 3 (cont'd). Experimental and theoretical crystal-field splittings of Nd^{3+} ion manifolds in YSAG

	Energy		$^{2S+1}L_J$ (centroid, cm^{-1})	Free ion mixture (%)
	Exp	Theo		
37	13,367	13,361		$88.58\,^4F_{7/2} + 4.65\,^4F_{5/2} + 2.21\,^4S_{3/2}$
38	13,441	13,451	$^4F_{7/2}$	$87.90\,^4F_{7/2} + 4.68\,^4S_{3/2} + 3.09\,^4F_{5/2}$
39	13,570	13,562	(13,490)	$58.76\,^4S_{3/2} + 39.38\,^4F_{7/2} + 0.58\,^4G_{5/2}$
40	13,580	13,588		$95.55\,^4S_{3/2} + 2.90\,^4F_{7/2} + 0.41\,^2H_{11/2}$
41	13,602	13,594	$^4S_{3/2}$	$63.68\,^4F_{7/2} + 35.15\,^4S_{3/2} + 0.28\,^2H_{11/2}$
42	13,642	13,647	(13,588)	$98.04\,^4F_{7/2} + 0.58\,^4S_{3/2} + 0.36\,^4I_{15/2}$
43	14,630	14,650		$98.65\,^4F_{9/2} + 1.60\,^4F_{7/2} + 0.57\,^4F_{5/2}$
44	14,695	14,696	$^4F_{9/2}$	$96.21\,^4F_{9/2} + 2.28\,^4F_{7/2} + 0.60\,^4F_{5/2}$
45	14,786	14,794	(14,756)	$97.14\,^4F_{9/2} + 0.97\,^2H_{11/2} + 0.63\,^2G_{7/2}$
46	14,834	14,820		$97.51\,^4F_{9/2} + 0.99\,^2H_{11/2} + 0.59\,^2G_{7/2}$
47	14,939	14,924		$98.18\,^4F_{9/2} + 1.23\,^2G_{7/2} + 0.16\,^4F_{7/2}$
48	15,770[a]	15,892		$97.34\,^2H_{11/2} + 2.11\,^2G_{7/2} + 0.27\,^4G_{5/2}$
49	15,860[a]	15,930	$^2H_{11/2}$	$97.76\,^2H_{11/2} + 1.76\,^2G_{7/2} + 0.19\,^4F_{9/2}$
50	15,886[a]	15,959	(15,971)	$98.95\,^2H_{11/2} + 0.39\,^2G_{7/2} + 0.21\,^2H_{9/2}$
51	15,964	15,964		$98.68\,^2H_{11/2} + 0.53\,^2G_{7/2} + 0.32\,^4F_{9/2}$
52	16,093[a]	16,022		$96.11\,^2H_{11/2} + 1.97\,^2G_{7/2} + 1.05\,^4F_{9/2}$
53	16,124[a]	16,067		$96.69\,^2H_{11/2} + 1.30\,^4F_{9/2} + 1.15\,^2G_{7/2}$
54	16,880	16,893		$56.29\,^4G_{5/2} + 41.53\,^2G_{7/2} + 1.34\,^2H_{11/2}$
55	17,010	17,000	$^4G_{5/2}$	$86.51\,^4G_{5/2} + 10.87\,^2G_{7/2} + 0.74\,^4S_{3/2}$
56	17,065	17,067	(17,090)	$73.89\,^4G_{5/2} + 22.91\,^2G_{7/2} + 0.98\,^2H_{11/2}$
57	17,262	17,231		$93.32\,^2G_{7/2} + 2.87\,^4G_{5/2} + 2.14\,^2H_{11/2}$
58	17,286	17,303	$^2G_{7/2}$	$95.89\,^2G_{7/2} + 1.81\,^2H_{11/2} + 1.56\,^4G_{5/2}$
59	17,331	17,341	(17,192)	$88.78\,^2G_{7/2} + 8.22\,^4G_{5/2} + 1.91\,^2H_{11/2}$
60	17,587[a]	17,664		$65.32\,^4G_{5/2} + 34.12\,^2G_{7/2} + 0.16\,^2H_{11/2}$

[a]Experimental energy levels not used in the crystal-field calculations.

2.5 Judd-Ofelt Theory

Application of Judd-Ofelt (JO) theory [20,21] has become a valuable model in predicting rare-earth laser performance. The model was first successfully applied to individual Stark levels in the ethylsulfate system by Axe [32] (Eu^{3+}) and by Krupke and Gruber [33] (Tm^{3+}). Since then JO theory has been used by numerous laboratories to calculate the branching ratios, radiative lifetimes, and eventually stimulated emission cross sections of the $^4F_{3/2} \rightarrow {}^4I_J$ (J = 9/2, 11/2, 13/2, 15/2) transitions. Detailed theoretical and experimental procedures are contained in works by Krupke [34,35], Weber [36], DeShazer [37,38], and Kaminskii [10,16]. The JO model is based on the following relationship: the line strength, $S(J,J')$, for a transition between an initial J manifold $|4f^n[SL]J\rangle$ and final J' manifold $|4f^n[S'L']J'\rangle$ can be written in the form

$$S(J,J') = \sum_{t=2,4,6} \Omega_t |\langle 4f^n[SL]J\|U^{(t)}\|4f^n[S'L']J'\rangle|^2 \qquad (2)$$

where $\langle\|U^{(t)}\|\rangle^2$ are the squares of the transition-matrix elements for intermediate coupling from the ground state to the excited manifold, and Ω_t are the three phenomenological JO parameters.

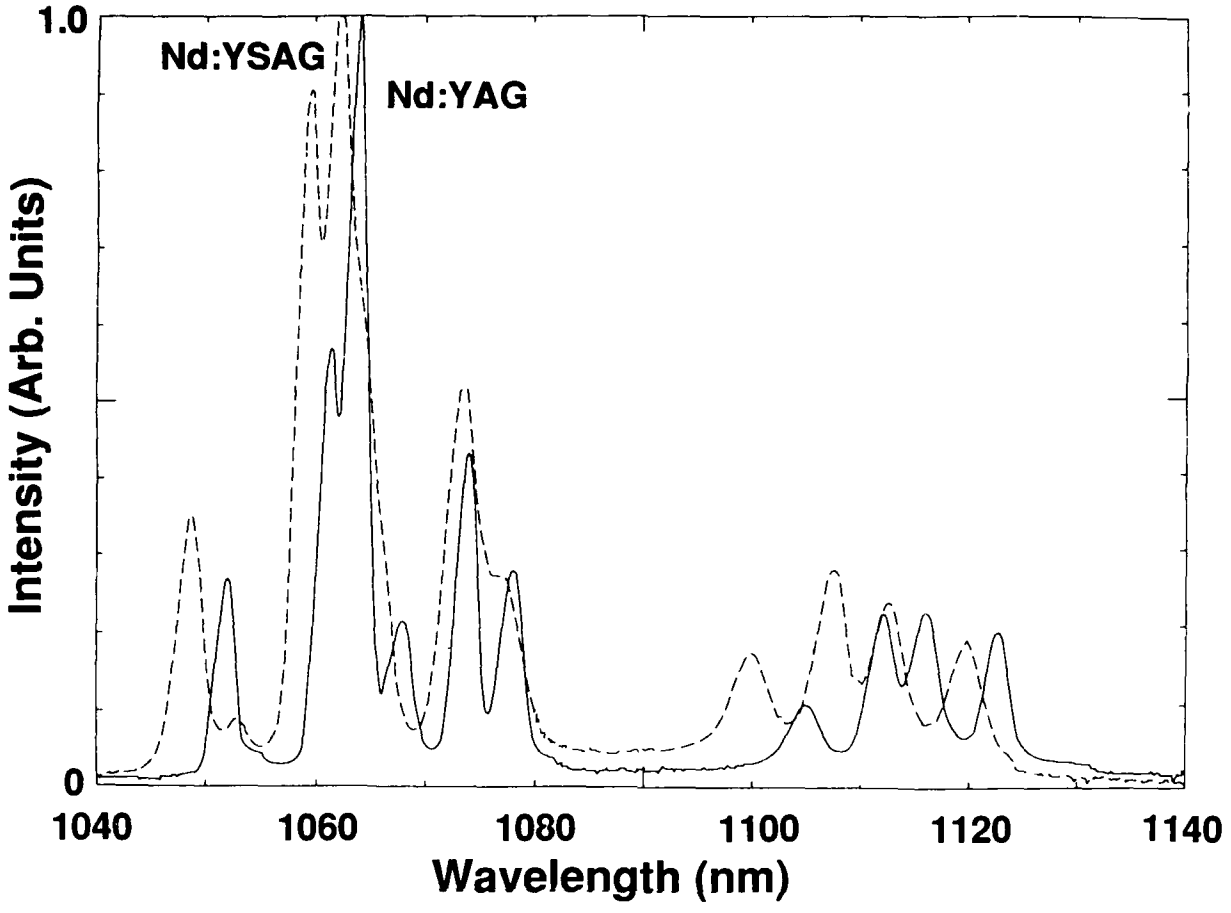

Figure 2. $^4F_{3/2} \rightarrow {}^4I_{11/2}$ fluorescence spectra of Nd^{3+} doped in YSAG and YAG at room temperature.

The numerical values of the transition-matrix elements for Nd^{3+} were taken from DeShazer [37].

In practice, the integrated absorption coefficient, $\Gamma = \int \alpha(\lambda)\, d\lambda$ emanating from the ground state (the $^4I_{9/2}$ manifold) was measured for 11 absorption bands using figure 1. The integrated absorption coefficient in turn is related to the line strength S by equation (3):

$$\Gamma = \frac{8\pi^3 N \bar{\lambda} e^2}{3ch(2J+1)} \frac{(n^2+2)^2}{9n} S(J,J') \qquad (3)$$

where N is the Nd^{3+} concentration, J is the total angular momentum quantum number of the initial level $\bar{\lambda}$ is the mean wavelength, and n is the index of refraction. The values for n were taken from Sellmeier's dispersion equation, equation (1). When the absorption band was a superposition of lines assigned to several inter-multiplet transitions, the matrix element was taken to be the sum of the corresponding squared matrix elements. The JO parameters were obtained by minimizing the sum of the squared differences between S_{meas} and S_{calc}. Table 4 shows Γ, n, S_{meas}, and S_{calc} for 11 absorption bands. The rms error of these calculations was 14 percent.

Once the JO parameters are known, S_{calc} was determined for transitions between $^4F_{3/2}$ and ^4I_J using the matrix elements emanating

Table 4. Absorption intensities for Nd:YSAG at 298 K

Excited state	Wavelength	n	Γ (nm/cm)	S_{meas}[a]	S_{calc}[a]
$^4F_{3/2}$	880	1.862	34.3	0.673	0.921
$^4F_{5/2}, ^2H_{9/2}$	805	1.865	159.2	3.408	3.177
$^4F_{7/2}, ^4S_{3/2}$	747	1.868	132.3	3.046	3.289
$^4F_{9/2}$	680	1.871	10.3	0.260	0.217
$^2H_{11/2}$	625	1.876	1.3	0.036	0.058
$^4G_{5/2}, ^2G_{7/2}$	583	1.880	75.8	2.213	2.242
$^4G_{7/2}, ^4G_{9/2}, ^2K_{13/2}$	520	1.888	50.9	1.655	1.253
$^2G_{9/2}, ^4G_{11/2}, ^2K_{15/2}, (^2D,^2P)_{3/2}$	470	1.897	17.4	0.621	0.310
$^2P_{1/2}, ^2D_{5/2}$	430	1.907	2.3	0.089	0.127
$^2P_{3/2}$	385	1.923	0.1	0.004	0.006
$^4D_{3/2}, ^4D_{1/2}, ^4D_{5/2}, ^2I_{11/2}$	357	1.936	35.0	1.593	1.733

[a]In units of 10^{-20} cm^2.
rms line strength of $S = 1.705 \times 10^{-20}$ cm^2.
rms deviation of line strength $(\Delta S)_{rms} = 0.239 \times 10^{-20}$ cm^2,
$(\Delta S)_{rms} = \{\Sigma(\Delta S^2)/(\text{No. of bands fitted} - \text{No. of parameters})\}^{1/2}$

from the metastable $^4F_{3/2}$ state [34]. The total spontaneous emission probability $A(J,J')$ was calculated from

$$A(J,J') = \frac{64\pi^4 e^2}{3h(2J+1)\bar{\lambda}^3}\frac{n(n^2+2)^2}{9}S(J,J') , \quad (4)$$

and the intermanifold branching ratio $\beta(J,J')$ is given by

$$\beta(J,J') = \frac{A(J,J')}{\Sigma A(J,J')} . \quad (5)$$

The JO parameters and the predicted branching ratios are given in table 5 for Nd:YSAG. For comparison, the JO parameters and both the predicted and experimentally determined branching ratios [39] for Nd:YAG are given. It is interesting to note that the experimental JO parameters are virtually the same for both YSAG and YAG. These results in turn yield comparable radiative lifetimes of the $^4F_{3/2}$ upper laser levels and branching ratios to the ^4I_J states.

Finally, the stimulated emission cross section σ_{21} for an inhomogeneously broadened linewidth (Gaussian lineshape) can be written as

$$\sigma_{21} = \frac{A_{21}\lambda^2}{4\pi n^2 \Delta\nu}\left(\frac{\ln 2}{\pi}\right)^{1/2} , \quad (6)$$

The transition probability for the laser transition $(2 \rightarrow 1)$ is given by

$$A_{21} = \frac{(1+\kappa)}{\kappa}\left(\frac{I_{21}}{I_T}\right)\tau_{rad}^{-1} , \quad (7)$$

where κ is the Boltzmann factor between the two levels of $^4F_{3/2}$, and I_{21}/I_T is the ratio of the photon rate for the laser transition to the photon rate of all transitions originating from either level of $^4F_{3/2}$. Using the value $\Delta\nu = 8$ cm^{-1} from the literature [10] and the experimentally determined values of $n = 1.86$, $\lambda = 1.0622 \times 10^{-4}$ cm, and $A_{21} = 780$ s^{-1}, we determine the value of $\sigma(R_2 \rightarrow Y_3)$ to be 4.0×10^{-19} cm^2.

2.6 Crystal-Field Calculations

The analysis of the experimental absorption data on Nd^{3+}:YSAG is the same as that of Nd^{3+}:LaLuGG given by Allik et al [40]. In these calculations, the experimentally determined Stark-level positions of Nd^{3+} given in table 3

Table 5. Experimental and calculated Judd-Ofelt parameters and predicted branching ratios for Nd^{3+}:YSAG and Nd^{3+}:YAG [16,34]

Note: Experimental branching ratios for Nd:YAG from reference 39 are given in square brackets.

	Values for Nd^{3+}:YSAG		Values for Nd^{3+}:YAG		
Judd-Ofelt parameters	Exp	Theo	Exp[a]	Exp[b]	Theo
Ω_2 (10^{-20} cm^2)	0.23	0.16	0.37	0.2	0.35
Ω_4 (10^{-20} cm^2)	2.87	1.79	2.29	2.7	2.36
Ω_6 (10^{-20} cm^2)	4.78	10.81	5.97	5.0	13.02
Radiative lifetime $^4F_{3/2}$ (μs)	250	173	259	261	128
Branching ratios (%)					
$\beta(^4F_{3/2} \rightarrow {}^4I_{9/2})$	37.8	23	32	37 [25]	21
$\beta(^4F_{3/2} \rightarrow {}^4I_{11/2})$	49.4	62	53	50 [60]	62
$\beta(^4F_{3/2} \rightarrow {}^4I_{13/2})$	12.4	15	15	13 [15]	16
$\beta(^4F_{3/2} \rightarrow {}^4I_{15/2})$	0.4	—	—	—	1

[a]Reference 16.
[b]Reference 34.

were used along with the free-ion Russell-Saunders $[SL]J$ states with the free-ion Hamiltonian containing the Coulomb, spin-orbit, L^2, $G(G_2)$, and $G(R_7)$ interactions [41]. The phenomenological crystal-field parameters were obtained by a least-squares fit of the calculated energy levels to the experimental energy levels. The theoretical energy levels were obtained using the crystal-field Hamiltonian

$$H_{CEF} = \sum_{ikq} B^*_{kq} C_{kq}(\hat{r}_i) \ , \qquad (8)$$

with $k = 2, 4, 6$ and $-k \le q \le k$. The B_{kq} are the crystal-field parameters, and the $C_{kq}(\hat{r})$ are spherical tensors. The sum on i in equation (8) covers the three electrons in the $4f^3$ electronic configuration of Nd^{3+}. Since we assume that the Nd^{3+} ions occupy the dodecahedral site with D_2 symmetry, the crystal-field parameters can be chosen real; thus there is a total of nine even-k B_{kq}. In this fitting, 9 out of 60 experimental levels were discarded because attempts to fit these levels were unsuccessful.

The positions of the energy levels of Nd:YSAG are quite similar to those of Nd:YAG; consequently, the crystal-field parameters of the latter [17] were chosen as starting parameters in the least-squares fitting. The resulting parameters that gave the best fit in units of cm^{-1} are

$$B_{20} = 588, \quad B_{22} = 40.8, \quad B_{40} = -192,$$
$$B_{42} = -1877, \quad B_{44} = -1194, \quad B_{60} = -1620,$$
$$B_{62} = -805, \quad B_{64} = 797, \quad B_{66} = -612,$$

with an rms deviation of 9.1 cm^{-1}.

As pointed out by Leavitt [42], the concept of rotational invariance is a convenient measure of the overall strength of the crystal field for comparison of the resulting B_{kq} for the same ion in different crystals. Here we define the rotational invariants, S_k, by

$$S_k = \left(\sum_{q=-k}^{k} B^*_{kq} B_{kq} \right)^{1/2} \qquad (9)$$

for $k = 2, 4$, and 6. The values of S_k for Nd:YAG [17] and those computed for Nd:YSAG are S_2(YAG) = 545 cm^{-1}, S_2(YSAG) = 591 cm^{-1}, S_4(YAG) = 3159 cm^{-1}, S_4(YSAG) = 3152 cm^{-1}, S_6(YAG) = 2548 cm^{-1}, S_6(YSAG) = 2437 cm^{-1}.

Initially, these results are rather surprising in view of the difference in cell size of YAG

(a = 12.000 Å) and YSAG (a = 12.271 Å), which would predict that the YAG crystal-field parameters would be much larger than those of YSAG. However, the distances from the yttrium site to the nearest oxygens are, for YAG, 2.303 Å (×4) and 2.432 Å (×4), and for YSAG, 2.338 Å (×4) and 2.440 Å (×4). Since these values are very similar, it is not surprising that the rotational invariants are comparable if it is assumed that the crystal-field parameters are predominately determined by the nearest-neighbor oxygen ions.

In order to calculate the intensity of the electric dipole transitions, we need the odd-k crystal-field components, A_{kq} ($cm^{-1}/Å^k$). In the point-charge model, the crystal-field components are given by [43]

$$A_{kq} = -e^2 \sum_j \frac{q_j C_{kq}(\hat{R}_j)}{R_j^{k+1}} , \qquad (10)$$

where $\vec{R}_j$ is the location of the ion with charge q_j (in units of the electronic charge) relative to the rare-earth site. We assume that the charges on the individual ions are $q_Y = 3$, $q_{Sc} = 3$, and $q_{Al} = -5 - 4q_O$, with q_O being the charge on the oxygen ions (note that when q_O is taken at the valence value, –2, q_{Al} is at its valence value of 3). The choice of covalency effects between the oxygen and Al site was made based on the fact that the Al–O distance is very small, 1.77 Å, compared to any other inter-ionic distances (the next smallest distance, Sc–O, is 2.07 Å). In the point-charge model, the crystal-field parameters are given by

$$B_{kq} = \rho_k A_{kq} , \qquad (11)$$

where the ρ_k are radial factors given by Morrison and Leavitt [44]. Using the values of ρ_k for Nd^{3+}, a set of experimental A^e_{kq} was obtained from the B_{kq} values; these values are given in the top row of table 6. These experimental A^e_{kq} were used to obtain the best value of q_O that fit the A_{kq} obtained from equation (10). Based on a value of $q_O = -1.79$, the odd-k A_{kq} ($cm^{-1}/Å^k$) from equation (10) are

$A_{32} = 1102$,
$A_{52} = -2179$,
$A_{54} = 1211$,
$A_{72} = 71.40$,
$A_{74} = 152.9$, and
$A_{76} = -200.3$
(all these odd-k A_{kq} are imaginary).

Having obtained a set of crystal-field components A^e_{kq} by the above procedure, one can obtain a set of crystal-field components for the entire rare-earth series by using equation (11). These results are given in table 6. These B_{kq} can serve as starting parameters for fitting the spectra of any rare-earth ion in YSAG. We refer to the crystal-field parameters obtained by this process as smoothed B_{kq}, since the process is usually used when the experimental data are analyzed on two or more rare-earth ions, in which case the experimental B_{kq} are forced, to a certain degree of consistency, for the entire rare-earth series.

The best-fit B_{kq} and the resulting values of the odd-k A_{kq} were used to calculate the intensity of the electric- and magnetic-dipole transitions for the rare-earth series. A detailed discussion of this calculation is given by Leavitt and Morrison [45]. The resulting theoretical JO intensity parameters are given in table 7 for the rare earths. In addition, the theoretical JO parameters, manifold-to-manifold branching ratios, and radiative lifetimes of the $^4F_{3/2}$ state for Nd:YSAG and Nd:YAG are given in table 5.

The individual Stark-level line strengths for all the crystal-field split levels of the multiplets $^4I_{9/2}$ through $^2G_{9/2}$ were calculated. From these line strengths, the branching ratios for the two levels of the $^4F_{3/2}$ (E = 11,423 cm^{-1} (No. 27) and E = 11,523 cm^{-1} (No. 28)) to the lower ^4I_J ($9/2 \le J \le 15/2$) crystal-field split levels were determined. The line strengths of the magnetic dipole operators were found to be less than the corresponding electric dipole line strengths by two orders of magnitude in almost all the transitions and were ignored in the calculation. In table 8 we give the branching ratios from both levels of the $^4F_{3/2}$ state to all the levels below. The Sellmeier dispersion equation (eq (1)) was used to obtain these results.

Table 6. Experimental crystal-field component A_{kq} ($cm^{-1}/Å^k$) and smoothed crystal-field parameters B_{kq} (cm^{-1}) obtained from the B_{kq} of Nd:YSAG

Ion	B_{20}	B_{22}	B_{40}	B_{42}	B_{44}	B_{60}	B_{62}	B_{64}	B_{66}
A_{kq}	3447	239	-332	-3250	-2067	-1019	-506	501	-385
Ce	635	44	-251	-2449	-1558	-2386	-1186	1174	-902
Pr	605	42	-215	-2101	-1336	-1911	-950	940	-722
Nd	588	41	-192	-1877	-1194	-1620	-805	797	-612
Pm	579	40	-177	-1735	-1104	-1449	-720	713	-547
Sm	575	40	-168	-1641	-1044	-1346	-669	662	-509
Eu	574	40	-161	-1572	-1000	-1274	-633	627	-481
Gd	575	40	-155	-1513	-962	-1210	-601	595	-457
Tb	577	40	-149	-1459	-928	-1145	-569	563	-432
Dy	579	40	-144	-1411	-897	-1082	-537	532	-409
Ho	583	40	-140	-1370	-872	-1031	-512	507	-390
Er	588	41	-137	-1341	-853	-1001	-498	493	-378
Tm	594	41	-135	-1317	-838	-983	-489	484	-371
Yb	599	42	-131	-1280	-814	-929	-462	457	-351

Table 7. Calculated Judd-Ofelt intensity parameters Ω_k of rare-earth ions in Y site of $Y_3Sc_2Al_3O_{12}$

	JO intensity parameters (10^{-20} cm^2)		
Ion	Ω_2	Ω_4	Ω_6
Ce	0.3031	5.634	46.20
Pr	0.1696	2.846	19.70
Nd	0.1635	1.789	10.81
Pm	0.09461	1.392	8.309
Sm	0.08253	1.172	6.878
Eu	0.06529	0.9122	4.864
Gd	0.05109	0.7031	3.359
Tb	0.08921	1.131	8.146
Dy	0.0627	0.8209	5.055
Ho	0.05357	0.6590	3.691
Er	0.05137	0.6182	3.481
Tm	0.04996	0.5897	3.363
Yb	0.04291	0.4862	2.562

Table 8. Line-to-line branching ratios (%) of two levels of $^4F_{3/2}$ [27,28] to all levels of ^4I_j manifolds (j = 1–26).

Manifolds	j	E (cm^{-1})	$\beta_{27\to j}$	$\beta_{28\to j}$
$^4I_{9/2}$	1	0	5.8	1.2
	2	114	2.7	3.4
	3	183	1.9	5.3
	4	301	11.5	7.9
	5	823	0.3	0.3
$^4I_{11/2}$	6	1979	22.5	4.6
	7	2022	23.1	12.9
	8	2101	2.9	25.6
	9	2136	3.4	9.8
	10	2437	2.6	5.5
	11	2495	5.5	6.2
$^4I_{13/2}$	12	3905	3.8	4.8
	13	3929	4.0	2.4
	14	4029	2.2	3.7
	15	4044	2.5	2.9
	16	4411[a]	0.4	1.7
	17	4419	1.4	0.4
	18	4478	2.3	0.5
$^4I_{15/2}$	19	5766	0.1	0.4
	20	5797	0.0	0.3
	21	5927	0.3	0.1
	22	5981	0.4	0.1
	23	6544	0.0	0.0
	24	6560	0.1	0.0
	25	6622	0.1	0.1
	26	6711	0.2	0.0

[a]Theoretical level

2.7 Laser Experiments

A long-pulse laser performance study of Nd:YSAG at 1.06 μm was undertaken using diode array excitation in the side-pump configuration. A diode array capable of producing 475 W in a 300-μs pulse was used as the excitation source. Details of the diode array and experimental procedures have been published previously [1].

One rod and one straight-through slab were fabricated from the same 6.35-mm-diameter "cored out" stock material by Lightning Optical Corp. (Tarpon Springs, FL). Both materials were 15 mm in length and had appropriate HR and AR coatings centered at 1.06 μm applied on opposite ends. The rod was 6.35 mm in diameter with the barrel polished. The slab was 3 mm thick. AR and HR coatings centered at 808 nm were applied on the side surfaces of the slab and the rod barrel to maximize diode absorption.

Of the two samples, the slab yielded the better results. The presence of significant optical (index-of-refraction) distortions in both samples was quite evident when the laser cavity was being aligned with a HeNe laser. The rod had an extremely high threshold, and laser oscillation could only be detected with a 99.9-percent output coupler at an input power of 360 W. The improved performance (lower threshold) of the slab may be attributed to the better geometrical coupling of the two-dimensional diode array to the slab than to the rod. The optical slope efficiencies and extrapolated thresholds for various reflectivity output couplers are shown in table 9 for the slab. The round-trip (Findlay-Clay) resonator loss was 20.2 ± 0.2 percent.

Table 9. Laser slope efficiencies and thresholds for Nd:YSAG using side-pump diode array excitation

Output coupler reflectivity	Optical slope efficiency (%)	Extrapolated threshold (mJ)
0.975 (∞)	4.2	48.1
0.965 (∞)	4.6	50.0
0.961 (∞)	5.1	52.0
0.908 (∞)	5.6	63.2
0.975 (63.5 cm)	7.6	47.0
0.950 (63.5 cm)	9.2	53.9
0.915 (75.0 cm)	8.4	55.1

3. Summary and Conclusions

The Judd-Ofelt intensity parameters for Nd:YSAG have been established by two different approaches. The first treats the parameters as phenomenological and adjusts them by directly fitting them to the experimentally measured line strengths. The second approach uses the results of a point-charge electrostatic model to predict values for the odd-k A_{kq} terms in the crystal-field expansion and then calculates a set of predicted intensities. Through a least-squares fitting subroutine, the predicted and observed intensities are reconciled, and a set of JO parameters is then calculated.

Overall good agreement between observed and calculated intensities eludes both approaches for several reasons. The model does not include dynamic lattice contributions or strain-broadening effects. The measured lifetimes usually include nonradiative contributions in emission. In absorption, multiple (minority) site absorption and phonon sidebands contribute to the measured absorption cross section. For example, in the experimental (first) method, S_{calc} from the ground state to the $^4F_{3/2}$ manifold is larger than S_{meas} for both YAG

and YSAG. This leads to a 20-percent error in the calculated branching ratio to the ^4I_j manifolds in Nd:YAG [34]. On the other hand, this method does predict the radiative lifetime of the $^4F_{3/2}$ state very well, provided the Nd concentration can be accurately determined. The theoretical (second) method predicts too small a radiative lifetime for the metastable state but does predict very well the manifold-to-manifold and line-to-line Stark transitions (see table 6 and compare table 8 to fig. 2). Additional comparisons of these two models have been published for Nd^{3+} in Y_2O_3 [46].

Slope efficiencies of 47 percent have been obtained for Nd:YAG using a diode array in the side-pump configuration with thresholds of approximately 20 mJ [1]. Under similar conditions, our present Nd:YSAG crystal obtained a best slope efficiency of only 9.2 percent. This is due to the much poorer optical quality of the crystal than is found for Nd:YAG. At high Nd^{3+} concentrations, Nd:YSAG has the advantage over Nd:YAG because the fluorescence lifetime is longer. The lower nonradiative transition rate of Nd:YSAG versus Nd:YAG can be attributed to greater distance between Nd ion pairs in YSAG. This yields fewer ion/ion interactions which quench the fluorescence. Thus, if more effort can be given to improving the optical quality of YSAG, as has been done for YAG, the Nd:YSAG crystal is potentially a better Q-switch laser than Nd:YAG.

Acknowledgements

SAIC gratefully acknowledges financial support from the Center for Night Vision and Electro-Optics. The authors thank C. F. Campana for the crystal structure solution, R. Phillips and W. Hovis for the elemental analysis on YSAG, V. King for technical assistance in the lifetime determination, L. Thompson for polishing samples, and L. Merkle for reviewing the manuscript. JBG wishes to thank the American Society for Engineering Education for their support, and M. E. Hills, Chemistry Division, Naval Weapons Center, China Lake, CA, for many helpful discussions and encouragement.

References

1. T. H. Allik, W. W. Hovis, D. P. Caffey, and V. King, Opt. Lett. **14** (1989), 116 .
2. J. Berger, D. F. Welch, D. F. Scifres, W. Streifer, and P. Cross, Electron. Lett. **23** (1987), 669.
3. B. Zhou, T. J. Kane, G. J. Dixon, and R. L. Byer, Opt. Lett. **10** (1985), 62.
4. R. A. Fields, M. Birnbaum, and C. L. Fincher, Appl. Phys. Lett. **51** (1987), 1885.
5. F. Hanson and D. Haddock, Appl. Opt. **27** (1988), 80.
6. F. Hanson and G. Imthurn, IEEE J. Quantum Electron. **QE-24** (1988), 1811.
7. J. B. Gruber, M. E. Hills, C. A. Morrison, G. A. Turner, and M. R. Kokta, Phys. Rev. B2 **37** (1988), 8564.
8. R. Burnham and A. D. Hayes, Opt. Lett. **14** (1989), 27.
9. A. L. Denisov, E. V. Zharikn, A. I. Zagumennyi, S. P. Kalitin, V. A. Smirnov, A. I. Talybov, and I. A. Shcherbakov, Zh. Prikl. Spektrosk. **49** (1988), 430.
10. A. A. Kaminskii, *Laser Crystals*, Springer, New York (1981).
11. A. G. Avanesov, A. A. Danilov, A. L. Denisov, E. V. Zharikov, A. I. Zagumennyi, O. V. Kuz'min, M. Yu. Nikol'skii, V. G. Ostroumov, V. F. Pisarenko, Academician A. M. Prokhorov, V. A. Smirnov, I. T. Sorokina, E. V. Tumaev, and I. A. Shcherbakov, Sov. Phys. Dokl. **32** (1987), 665.

12. Kh. S. Bagdasarov, A. A. Kaminskii, A. M. Kevorkov, and A. M. Prokorov, Sov. Phys. Dokl. **19** (1975), 671.
13. M. Kokta, J. Solid State Chem. **8** (1973), 39.
14. C. D. Brandle and R. L. Barns, J. Crystal Growth **20** (1973), 1.
15. V. F. Kitaeva, E. V. Zharikov, and I. L. Chistyi, Phys. Status Solidi **a92** (1985), 475.
16. A. A. Kaminskii and L. Li, Phys. Status Solidi **a26** (1974), K21.
17. C. A. Morrison and R. P. Leavitt, "Spectroscopic Properties of Triply Ionized Lanthanides in Transparent Host Materials," in *Handbook of the Physics and Chemistry of Rare Earths*, Vol. 5, eds. K. A. Gschneidner, Jr., and L. Eyring, North-Holland, New York (1982), 461–684.
18. G. Huber, E. W. Duczynski, P. Mitzscherlich, and H. O. Teichmann, J. Phys. Paris **48** (1987), C7-309.
19. E. W. Duczynski, H. J. v.d. Heide, G. Huber, P. Mitzscherlich, K. Petermann, and H. O. Teichmann, in Conference on Lasers and Electro-Optics, Technical Digest Series 1989, Optical Society of America, Washington, DC (1989), paper TuJ58.
20. B. R. Judd, Phys. Rev. **127** (1962), 750.
21. G. S. Ofelt, J. Chem. Phys. **37** (1962), 511.
22. C. A. Morrison, N. Karayianis, and D. E. Wortman, *Rare-Earth Ion-Host Lattice Interactions, 4.—Predicting Spectra and Intensities of Lanthanides in Crystals*, Harry Diamond Laboratories, HDL-TR-1816 (June 1977).
23. L. G. Morozova and P. P. Feofilov, Izv. Akad. Nauk. SSSR, Neorg. Mater. **4** (1968), 1738.
24. C. D. Brandle and J. C. Vanderleeden, IEEE J. Quant. Electron. **QE-10**, No. 2 (1974), 67.
25. D. Pruss, G. Huber, A. Belmowski, V. V. Laptev, I. A. Shcherbakov, and Y. V. Zharikov, J. Appl. Phys. **B28** (1982), 355.
26. R. Phillips, Kevex Instruments, 50 Valley Stream Parkway, Malvern, PA, 19355 (unpublished).
27. G. A. Bogomolova, L. A. Bumagina, A. A. Kaminskii, and B. Z. Malkin, Sov. Phys. Solid State **19** (1977), 1428.
28. C. F. Campana, Nicolet X-ray Division, 5225-5 Verona Road, Madison, WI 53711 (unpublished).
29. W. L. Bond, J. Appl. Phys. **36** (1965), 1674.
30. S. H. Wemple and W. J. Tabor, J. Appl. Phys. **44** (1973), 1395.
31. J. B. Gruber, M. E. Hills, C. K. Jayasankar, F. S. Richardson, and T. H. Allik, *Energy Levels and Spin-Correlation Crystal Field Effects: Nd^{3+} ($4f^3$) in $Y_3Al_5O_{12}$, $Y_3Sc_2Al_3O_{12}$, $Gd_3Sc_2Ga_3O_{12}$, and $La_3Lu_2Ga_3O_{12}$*, manuscript in preparation.
32. J. D. Axe, J. Chem. Phys. **39** (1963), 1154.
33. W. F. Krupke and J. B. Gruber, Phys. Rev. **139** (1965), A2008.
34. W. F. Krupke, IEEE J. Quantum Electron. **QE-7** (1971), 153.
35. W. F. Krupke, IEEE J. Quantum Electron. **QE-10** (1974), 450.
36. M. J. Weber, T. E. Varitmos, and B. M. Matsinger, Phys. Rev. **B8** (1973), 47.
37. T. S. Lomheim and L. G. DeShazer, J. Appl. Phys. **49** (1978), 5517.
38. T. S. Lomheim and L. G. DeShazer, Phys. Rev. **B20** (1979), 4343.
39. E. Comperchio, M. Weber, and R. Monchamp, *High Quality Nd:YAG Laser Materials*, U.S. Army Electronics Command, Fort Monmouth, NJ, Final Report, Contract DAAB07-69-C-0227 (1970).
40. T. H. Allik, S. A. Stewart, D. K. Sardar, G. J. Quarles, R. C. Powell, C. A. Morrison, G. A. Turner, M. R. Kokta, W. W. Hovis, and A. A. Pinto, Phys. Rev. **B37** (1988), 9129.
41. B. G. Wybourne, *Spectroscopic Properties of Rare Earths*, Wiley, New York, (1965). [The free-ion parameters E^k, α, β, γ, and ζ are given in Ref. 40.]
42. R. P. Leavitt, J. Chem. Phys. **77** (1982), 1661.

43. C. A. Morrison, *Angular Momentum Theory Applied to Interactions in Solids*, Lecture Notes in Chemistry **47**, Springer-Verlag, New York (1988).
44. C. A. Morrison and R. P. Leavitt, J. Chem. Phys. **71** (1979), 2366.
45. R. P. Leavitt and C. A. Morrison, J. Chem. Phys. **73** (1980), 749.
46. C. A. Morrison, R. P. Leavitt, J. B. Gruber, and N. C. Chang, J. Chem. Phys. **79** (1983), 4758.

DISTRIBUTION

ADMINISTRATOR
DEFENSE TECHNICAL INFORMATION CENTER
ATTN DTIC-DDA (12 COPIES)
CAMERON STATION, BUILDING 5
ALEXANDRIA, VA 22314-6145

DIRECTOR
NIGHT VISION & ELECTRO-OPTICS CENTER
ATTN TECHNICAL LIBRARY
ATTN R. BUSER
ATTN A. PINTO
ATTN J. HABERSAT
ATTN R. RHODE
ATTN W. TRESSEL
FT BELVOIR, VA 22060

DIRECTOR
DEFENSE NUCLEAR AGENCY
ATTN TECH LIBRARY
WASHINGTON, DC 20305

UNDER SECRETARY OF DEFENSE RES
& ENGINEERING
ATTN TECHNICAL LIBRARY, 3C128
WASHINGTON, DC 20301

OFFICE OF THE DEPUTY CHIEF OF STAFF,
FOR RESEARCH, DEVELOPMENT, &
ACQUISITION
DEPARTMENT OF THE ARMY
ATTN DAMA-ARZ-B, I. R. HERSHNER
WASHINGTON, DC 20310

COMMANDER
US ARMY ARMAMENT MUNITIONS &
CHEMICAL COMMAND (AMCCOM)
US ARMY ARMAMENT RESEARCH &
DEVELOPMENT CENTER
ATTN DRDAR-TSS, STINFO DIV
DOVER, NJ 07801

COMMANDER
ATMOSPHERIC SCIENCES LABORATORY
ATTN TECHNICAL LIBRARY
WHITE SANDS MISSILE RANGE, NM 88002

DIRECTOR
US ARMY BALLISTIC RESEARCH LABORATORY
ATTN SLCBR-DD-T (STINFO)
ABERDEEN PROVING GROUND, MD 21005

DIRECTOR
US ARMY ELECTRONICS WARFARE
LABORATORY
ATTN J. CHARLTON
ATTN DELET-DD
FT MONMOUTH, NJ 07703

COMMANDING OFFICER
USA FOREIGN SCIENCE & TECHNOLOGY CENTER
FEDERAL OFFICE BUILDING
ATTN DRXST-BS, BASIC SCIENCE DIV
CHARLOTTESVILLE, VA 22901

COMMANDER
US ARMY MATERIALS & MECHANICS
RESEARCH CENTER
ATTN DRXMR-TL, TECH LIBRARY
WATERTOWN, MA 02172

US ARMY MATERIEL COMMAND
5001 WISENHOWER AVE
ALEXANDRIA, VA 22333-0001

US ARMY MATERIEL SYSTEMS ANALYSIS
ACTIVITY
ATTN DRXSY-MP (LIBRARY)
ABERDEEN PROVING GROUND, MD 21005

COMMANDER
US ARMY MISSILE & MUNITIONS
CENTER & SCHOOL
ATTN ATSK-CTD-F
ATTN DRDMI-TB, REDSTONE SCI INFO CENTER
REDSTONE ARSENAL, AL 35809

COMMANDER
US ARMY RESEARCH OFFICE (DURHAM)
ATTN J. MINK
ATTN M. STROSIO
ATTN M. CIFTAN
ATTN B. D. GUENTHER
PO BOX 12211
RESEARCH TRIANGLE PARK, NC 27709

COMMANDER
US ARMY RSCH & STD GRP (EUROPE)
FPO NEW YORK 09510

COMMANDER
US ARMY TEST & EVALUATION COMMAND
ATTN D. H. SLINEY
ATTN TECH LIBRARY
ABERDEEN PROVING GROUND, MD 21005

COMMANDER
US ARMY TROOP SUPPORT COMMAND
ATTN DRXRES-RTL, TECH LIBRARY
NATICK, MA 01762

OFFICE OF NAVAL RESEARCH
ATTN J. MURDAY
ARLINGTON, VA 22217

DIRECTOR
NAVAL RESEARCH LABORATORY
ATTN CODE 2620, TECH LIBRARY BR
ATTN G. QUARLES
ATTN G. KINTZ
ATTN A. ROSENBAUM
ATTN G. RISENBLATT
ATTN CODE 5554, F. BARTOLI
ATTN CODE 5554, L. ESTEROWITZ
ATTN CODE 5554, R. E. ALLEN
WASHINGTON, DC 20375

COMMANDER
NAVAL WEAPONS CENTER
ATTN CODE 3854, R. SCHWARTZ
ATTN CODE 3854, M. HILLS
ATTN CODE 3844, M. NADLER
ATTN CODE 385, R. L. ATKINS
ATTN CODE 343, TECHNICAL INFORMATION DEPARTMENT
CHINA LAKE, CA 93555

AIR FORCE OFFICE OF SCIENTIFIC RESEARCH
ATTN MAJOR H. V. WINSOR, USAF
BOLLING AFB
WASHINGTON, DC 20332

HQ, USAF/SAMI
WASHINGTON, DC 20330

DEPARTMENT OF COMMERCE
NATIONAL BUREAU OF STANDARDS
ATTN LIBRARY
WASHINGTON, DC 20234

NASA LANGLEY RESEARCH CENTER
ATTN N. P. BARNES (2 COPIES)
ATTN G. ARMAGAN
ATTN P. CROSS
ATTN D. GETTENY
ATTN J. BARNES
ATTN E. FILER
ATTN C. BAIR
ATTN N. BOUNCRISHANI
HAMPTON, VA 23665

DIRECTOR
ADVISORY GROUP ON ELECTRON DEVICES
ATTN SECTRY, WORKING GROUP D
210 VARICK STREET
NEW YORK, NY 10013

AEROSPACE CORPORATION ATTN M. BIRNBAUM
ATTN N. C. CHANG
ATTN T. S. ROSE
PO BOX 92957
LOS ANGELES, CA 90009

ALLIED ADVANCED APPLICATION DEPT
ATTN A. BUDGOR
31717 LA TIEMDA DRIVE
WESTLAKE VILLAGE, CA 91362

ALLIED SIGNAL INC.
ATTN Y. BAND
ATTN R. MORRIS
POB 1021R
MORRISTOWN, NJ 07960

AMES LABORATORY DOE
IOWA STATE UNIVERSITY
ATTN K. A. GSCHNEIDNER, JR. (2 COPIES)
AMES, IA 50011

ARGONNE NATIONAL LABORATORY
ATTN W. T. CARNALL
9700 SOUTH CASS AVENUE
ARGONNE, IL 60439

BOOZ, ALLEN AND HAMILTON
ATTN W. DROZDOSKI
4330 EAST WEST HWY
BETHESDA, MD 20814

BRIMROSE CORP OF AMERICA
ATTN R. G. ROSEMEIER
7527 BELAIR ROAD
BALTIMORE, MD 21236

DRAPER LAB
ATTN F. HAKIMI
MS 53
555 TECH. SQ
CAMBRIDGE, MA 02139

ENGINEERING SOCIETIES LIBRARY
ATTN ACQUISITIONS DEPT
345 EAST 47TH STREET
NEW YORK, NY 10017

FIBERTECH INC.
ATTN H. R. VERDIN (3 COPIES)
510-A HERNDON PKWY
HERNDON, VA 22070

HUGHES AIRCRAFT COMPANY
ATTN D. SUMIDA
3911 MALIBU CANYON RD
MALIBU, CA 90265

DISTRIBUTION (cont'd)

IBM RESEARCH DIVISION
ALMADEN RESEARCH CENTER
ATTN R. M. MACFARLANE
MAIL STOP K32 802(D)
650 HARRY ROAD
SAN JOSE, CA 95120

DIRECTOR
LAWRENCE RADIATION LABORATORY
ATTN M. J. WEBER
ATTN H. A. KOEHLER
ATTN W. KRUPKE
LIVERMORE, CA 94550

MARTIN MARIETTA
ATTN F. CROWNE
ATTN J. LITTLE
ATTN WORCHESKY
ATTN D. WORTMAN
1450 SOUTH ROLLING ROAD
BALTIMORE, MD 21227

MIT LINCOLN LAB
ATTN B. AULL
PO BOX 73
LEXINGTON, MA 02173

DEPARTMENT OF MECHANICAL, INDUSTRIAL, &
AEROSPACE ENGINEERING
PO BOX 909
ATTN S. TEMKIN
PISCATAWAY, NJ 08854

NATIONAL OCEANIC & ATMOSPHERIC ADM
ENVIRONMENTAL RESEARCH LABS
ATTN LIBRARY, R-51, TECH RPTS
BOULDER, CO 80302

OAK RIDGE NATIONAL LABORATORY
ATTN R. G. HAIRE
OAK RIDGE, TN 37830

W. J. SCHAFER ASSOC.
ATTN J. W. COLLINS
321 BILLERICA ROAD
HELMSFORD, MA 01824

SCIENCE APPLICATIONS, INTERNATIONAL CORP
ATTN T. ALLIK (10 COPIES)
1710 GOODRIDGE DRIVE
McLEAN, VA 22102

UNION CARBIDE CORP
ATTN M. R. KOKTA (10 COPIES)
ATTN J. H. W. LIAW
750 SOUTH 32ND STREET
WASHOUGAL, WA 98671

ARIZONA STATE UNIVERSITY
DEPT OF CHEMISTRY
ATTN L. EYRING
TEMPE, AZ 85281

CARNEGIE MELLON UNIVERSITY
SCHENLEY PARK
ATTN PHYSICS & EE, J. O. ARTMAN
PITTSBURGH, PA 15213

COLORADO STATE UNIVERSITY
PHYSICS DEPARTMENT
ATTN S. KERN
FORT COLLINS, CO 80523

UNIVERSITY OF CONNECTICUT
DEPARTMENT OF PHYSICS
ATTN R. H. BARTRAM
STORRS, CT 06269

UNIVERSITY OF SOUTH FLORIDA
PHYSICS DEPT
ATTN R. CHANG
ATTN SENGUPTA
TAMPA, FL 33620

JOHNS HOPKINS UNIVERSITY
DEPT OF PHYSICS
ATTN B. R. JUDD
BALTIMORE, MD 21218

KALAMAZOO COLLEGE
DEPT OF PHYSICS
ATTN K. RAJNAK
KALAMAZOO, MI 49007

MASSACHUSETTS INISTITUTE OF TECHNOLOGY
CRYSTAL PHYSICS LABORATORY
ATTN H. P. JENSSEN
ATTN A. LINZ
CAMBRIDGE, MA 02139

MASSACHUSETTS INSTITUTE OF TECHNOLOGY
ATTN V. BAGNATO
ROOM 26-251
77 MASS AVE
CAMBRIDGE, MA 02139

UNIVERSITY OF MINNESOTA, DULUTH
DEPARTMENT OF CHEMISTRY
ATTN L. C. THOMPSON
DULUTH, MN 55813

DISTRIBUTION (cont'd)

OKLAHOMA STATE UNIVERSITY
DEPT OF PHYSICS
ATTN R. C. POWELL
STILLWATER, OK 74078

PENNSYLVANIA STATE UNIVERSITY
MATERIALS RESEARCH LABORATORY
ATTN W. B. WHITE
UNIVERSITY PARK, PA 16802

PRINCETON UNIVERSITY
DEPARTMENT OC CHEMISTRY
ATTN D. S. McCLURE
PRINCETON, NJ 08544

SAN JOSE STATE UNIVERSITY
DEPARTMENT OF PHYSICS
ATTN J. B. GRUBER (10 COPIES)
SAN JOSE, CA 95192

SETON HALL UNIVERSITY
CHEMISTRY DEPARTMENT
ATTN H. BRITTAIN
SOUTH ORANGE, NJ 07099

UNIVERSITY OF VIRGINIA
DEPT OF CHEMISTRY
ATTN DR. F. S. RICHARDSON (2 COPIES)
ATTN DR. M. REID
CHARLOTTESVILLE, VA 22901

UNIVERSITY OF WISCONSIN
CHEMISTRY DEPARTMENT
ATTN J. WRIGHT
ATTN B. TISSUE
MADISON, WI 62705

US ARMY LABORATORY COMMAND
ATTN TECHNICAL DIRECTOR, AMSLC-CT

INSTALLATION SUPPORT LABORATORY
ATTN LEGAL OFFICE, SLCIS-CC
ATTN S. ELBAUM, SLCIS-CC

USAISC
ATTN TECHNICAL REPORTS
BRANCH, AMSLC-IM-TR (2 COPIES)

HARRY DIAMOND LABORATORIES
ATTN D/DIVISION DIRECTORS
ATTN LIBRARY, SLCHD-TL (3 COPIES)
ATTN LIBRARY, SLCHD-TL (WOODBRIDGE)
ATTN CHIEF, SLCHD-NW-E
ATTN CHIEF, SLCHD-NW-EP
ATTN CHIEF, SLCHD-NW-EH
ATTN CHIEF, SLCHD-NW-ES
ATTN CHIEF, SLCHD-NW-R
ATTN CHIEF, SLCHD-NW-TN
ATTN CHIEF, SLCHD-NW-RP
ATTN CHIEF, SLCHD-NW-CS
ATTN CHIEF, SLCHD-NW-TS
ATTN CHIEF, SLCHD-NW-RS
ATTN CHIEF, SLCHD-NW-P
ATTN CHIEF, SLCHD-NW-PO
ATTN CHIEF, SLCHD-ST-C
ATTN CHIEF, SLCHD-ST-RS
ATTN CHIEF, SLCHD-TT
ATTN KENYON, C. S., SLCHD-NW-EP
ATTN MILETTA, J. R., SLCHD-NW-EP
ATTN McLEAN, F. B., SLCHD-NW-RP
ATTN LIBELO, L., SLCHD-ST-MW
ATTN BENCIVENGA, A. A., SLCHD-ST-SP
ATTN SATTLER, J., SLCHD-CS
ATTN NEMARICH, J., SLCHD-ST-SP
ATTN WEBER, B., SLCHD-ST-CB
ATTN BAHDER, T., SLCHD-ST-AP
ATTN BENCIVENGA, B., SLCHD-TA-AS
ATTN BRUNO J., SLCHD-ST-AP
ATTN DROPKIN. H., SLCHD-ST-AP
ATTN EDWARDS A., SLCHD-ST-AP
ATTN HAY G., SLCHD-ST-AP
ATTN LEAVITT, R., SLCHD-ST-AP
ATTN PHAM, J., SLCHD-ST-AP
ATTN SIMONIS, G., SLCHD-ST-AP
ATTN STEAD, M., SLCHD-ST-AP
ATTN STELLATO, J., SLCHD-ST-AP
ATTN TOBIN, M., SLCHD-ST-AP
ATTN TOBER, R., SLCHD-ST-AP
ATTN TURNER, G., SLCHD-ST-AP
ATTN WORTMAN, D., SLCHD-ST-AP
ATTN GARVIN, C., SLCHD-ST-SS
ATTN GOFF, J., SLCHD-ST-SS
ATTN MORRISON C., SLCHD-ST-AP (10 COPIES)